ACS APPLIED MATERIALS & INTERFACES

RESEARCH ARTICLE

www.acsami.org

Oligoselenophene Derivatives Functionalized with a Diketopyrrolopyrrole Core for Molecular Bulk Heterojunction Solar Cells

Katherine A. Mazzio, Mingjian Yuan, Ken Okamoto, and Christine K. Luscombe*

Materials Science and Engineering Department, University of Washington, Seattle, Washington 98195-2120, United States

ABSTRACT: Solution-processable oligoselenophenes functionalized with diketopyrrolopyrrole cores have been synthesized for use as the donor material in bulk heterojunction solar cells. The optical absorption of these materials extends to the edge of the visible spectrum. Power conversion efficiencies of 1.53 ± 0.04% for DPPS and 0.84 ± 0.04% for DPPDS were obtained under simulated 100 mW/cm^2 AM 1.5G irradiation for devices when $PC_{61}BM$ was used as an acceptor. DPPS showed hole mobilities of 4×10^{-5} cm^2/(V s) and a peak external quantum efficiency (EQE) of 25%, while DPPDS showed hole mobilities of 2×10^{-5} cm^2/(V s) and a peak EQE of 19%. To the best of our knowledge, these are the first oligoselenophenes that have been reported in molecular bulk heterojunction solar cells and this study could serve as a springboard for the design and optimization of high-performance selenophene-containing photovoltaics.

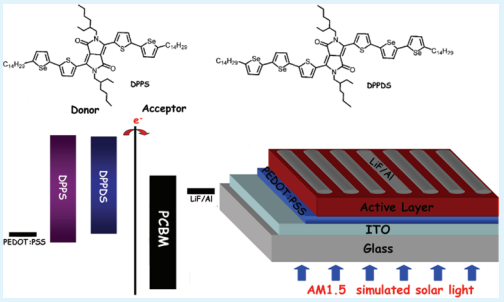

KEYWORDS: organic photovoltaics, bulk heterojunction solar cells, oligoselenophenes, small molecule semiconductors, organic electronics, organic field-effect transistors

INTRODUCTION

Conjugated polymer-based bulk heterojunction (BHJ) solar cells have received considerable attention as promising renewable energy resources.[1−3] Significant efforts are being put forth to improve the power conversion efficiencies (PCEs) in order to meet the demands for high performance photovoltaic applications.[4−7] PCEs as high as 7.7%[8] have been achieved using a low band gap polymer as the donor and a soluble fullerene derivative, (6,6)-phenyl C_{71}-butyric acid methyl ester ($PC_{71}BM$), as the acceptor; however, this efficiency is still lower than that required for commercial applications.[9] The strong motivation for approaching higher PCEs drives various research efforts in the area of BHJ solar cells.[10−16] Recently, much attention has been focused on solution processable small molecule semiconductors as alternatives to conjugated polymers in BHJ solar cells due to several intrinsic advantages.[17,18] In general, small molecule organic semiconductors exhibit higher hole and electron mobility than their polymeric counterparts because they are more likely to exhibit long-range order. In addition, small molecule semiconductors do not suffer from batch to batch variations, broad molecular weight distributions, or end group contamination during the syntheses.[19]

These benefits have resulted in a number of research groups investigating the application of small molecule based organic solar cells. To date, small molecule-based BHJ solar cell devices exhibit PCEs ranging from 0.3 to 4.4%, where the higher PCEs have been achieved using $PC_{71}BM$ as an acceptor rather than $PC_{61}BM$.[20−22] According to the literature, the majority of the donor materials have been focused on thiophene-based oligomers because of their high charge carrier mobility; however, thiophene-based oligomers often do not absorb strongly in the longer wavelengths of the solar spectrum and tend to exhibit low solubility in common organic solvents. This may result in lower PCEs in comparison to either polymer-based solar cells or thermally deposited small molecule bilayer solar cells.

Selenophenes are thought to compensate for some of the disadvantages of thiophene containing compounds. In general, selenophene containing compounds have the advantages of lower oxidation and reduction potentials, strong light absorptivity, ease of polarizability, and improved interchain charge transfer, while maintaining structural similarities to thiophenes.[23] Selenophene-based oligomers and polymers have attracted some interest as organic thin film transistor (OTFT) materials,[24,25] as several selenophene-containing compounds have been shown to exhibit excellent hole mobility. Despite these advantages, selenophene-based compounds have attracted little attention in the area of organic photovoltaics.[26,27] To the best of our knowledge, no oligoselenophene-based photovoltaic materials have been reported.

Additionally, diketopyrrolopyrrole (DPP)-based materials have attracted tremendous attention recently because of their promising performance in solar cells as well as in field-effect transistors.[28−33] The DPP core contains a planar bicyclic structure that promotes strong $\pi-\pi$ stacking providing high hole

Received: September 24, 2010
Accepted: December 7, 2010
Published: January 10, 2011

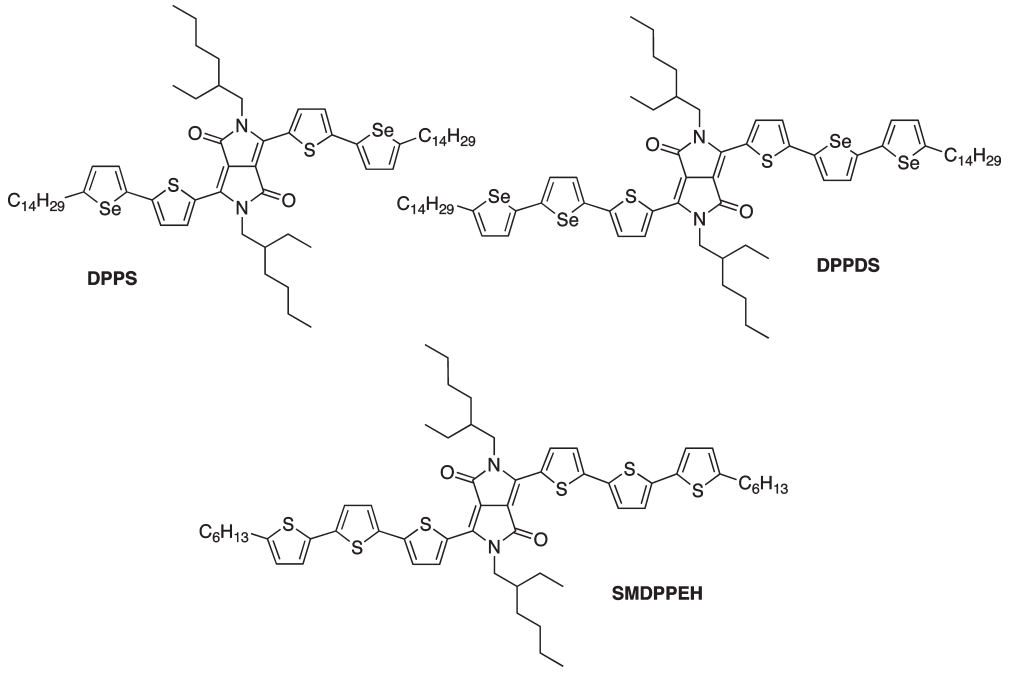

Figure 1. Structures of the synthesized oligoselenophenes, DPPS and DPPDS, and the previously synthesized SMDPPEH.

mobility materials.[34] It also contains electron-withdrawing carbonyl groups that make the DPP core suitable for use as the acceptor unit in low -band-gap donor−acceptor materials. These two properties make DPP-based materials attractive for use in photovoltaic devices.

The goal of this work was to synthesize selenophene derivatives of a previously synthesized thiophene-based material containing a DPP core (SMDPPEH) where a PCE of 3.0% was achieved using $PC_{71}BM$ as an acceptor.[22] Here, we report the synthesis of the oligoselenophene derivatives DPPS and DPPDS as shown in Figure 1, containing a DPP core for solution processable small molecule-based BHJ solar cells. It was necessary to increase the solubilizing chain from a C6 alkyl chain to a C14 alkyl chain because of the limited solubility observed in the selenophene derivatives. The aim in designing these systems was to take advantage of the hole transporting and electron donating characteristics of these oligoselenophenes. It was hoped that the internal electron transfer between the selenophene and DPP core would induce a stronger light absorption in long wavelengths compared to the thiophene derivatives, and that the higher molecular ordering of oligoselenophenes and DPP-based materials in the solid state may potentially lead to enhanced charge carrier mobilities. To the best of our knowledge, this work represents the first reported example of oligoselenophenes to be used in molecular bulk heterojunction devices, and this work can be used as a basis for improving upon future oligoselenophene-based systems.

RESULTS AND DISCUSSION

1. Synthesis and Structure. Scheme 1 depicts the synthesis and structures of the compounds studied here. Compounds DPPS and DPPDS were synthesized using the Stille cross-coupling reaction. Different length selenophene oligomers were obtained by using step-by-step Stille cross-coupling reactions. The dibrominated DPP core (**7**) was then treated with 2.5 equiv. of the appropriate selenophene trimethyltin compound (**4**) or (**6**), giving DPPS as a deep red powder and DPPDS as a deep blue powder. All of the materials were purified by column chromatography and were characterized by ^{1}H NMR, ^{13}C NMR, and mass spectroscopy. All the materials were soluble in common solvents such as chloroform, toluene, and chlorobenzene.

2. Density Funtional Theory (DFT) Calculations. The geometries and electronic structures of methyl analogues of DPPS and DPPDS were analyzed with Gaussian 03 software. Becke's three-parameter gradient-corrected functional (B3LYP) with a polarized 6-31G(d) basis was used for full geometry optimization. Methyl groups were used in approximation of long alkyl chains in order to limit calculation time. The highest occupied molecular orbital (HOMO) and lowest unoccupied molecular orbital (LUMO) surface plots of the ground-state optimized structures are illustrated in Figure 2. DFT calculated HOMO and LUMO energies are summarized in Table 1. In these compounds, both the HOMO and LUMO are delocalized over the entire molecule. The calculated HOMO and LUMO energy levels of the ground state optimized geometry for compound DPPS are −4.95 and −3.05 eV, respectively. The difference between the ground HOMO and LUMO energies were then used to estimate the theoretical energy gap of DPPS, which is 1.90 eV. This value is in agreement with electrochemical observations for DPPS (Figure 3, Table 1). The DFT calculation indicates that the HOMO energy level rises with increasing selenophene units due to the increase in π-conjugation length. The LUMO energy level is effectively stabilized by the addition of selenophene units. The calculated ground-state energy gap for DPPDS was found to be 1.79 eV, which is also in agreement with the data obtained from electrochemistry.

The calculated potential energy minima, the computed bond lengths and angles of a series of DPP derivatives are summarized in Table 2. The computed geometry agrees well with experimental geometry of the DPP core.[35] The main difference between the computed geometries is in the side thiophene and selenophene

Scheme 1. Synthesis Routes of Target Molecules[a]

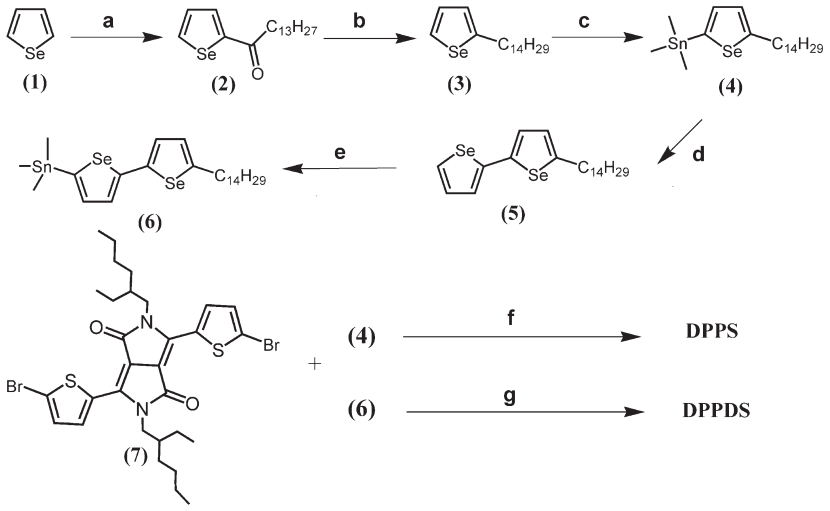

[a] (a) $AlCl_3$, myristoyl chloride, anhydrous CH_2Cl_2; (b) $AlCl_3$, $LiAlH_4$; (c) n-butyllithium, THF, trimethyltin chloride; (d) 2-bromoselenophene, $Pd(PPh_3)_2Cl_2$, toluene, nitrogen; (e) n-butyllithium, THF, trimethyltin chloride; (f) 2-bromoselenophene, $Pd(PPh_3)_2Cl_2$, toluene, nitrogen; (g) dibromo-DPP (7), $Pd(PPh_3)_2Cl_2$, toluene, nitrogen.

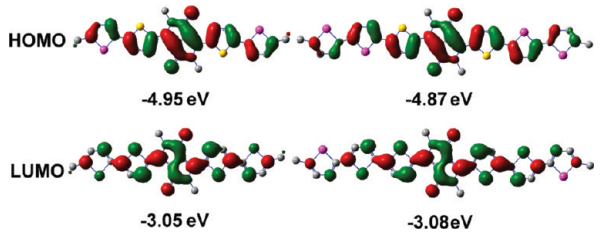

Figure 2. HOMO and LUMO surface plots for methyl-substituted analogues of DPPS and DPPDS.

oligomer chain planarity, where an increase in planarity is observed as the number of selenophene units is increased. It has previously been reported that oligoselenophenes are more planar than the corresponding oligothiophenes.[36,37] The computed geometry of DPPDS in particular agrees well with prior work,[36,37] showing torsion angles of 0.67°, 179.46°, and 179.97 for for C_1-C_2-C_4-C_5, C_6-C_7-C_8-C_9, and C_{10}-$C_{11}-C_{12}$-C_{13}, respectively.

3. Electrochemistry. Electrochemical cyclic voltammetry (CV) was employed to investigate the redox behavior of the two oligomers and to estimate their HOMO and LUMO energy levels. All of the cyclic voltammetry (CV) processes were carried out in anhydrous dichloromethane. The HOMO and LUMO energy levels were calculated from the half-wave potentials of the oxidation peaks (E_{ox}) and reduction peaks (E_{red}) vs Ag/Ag^+,[38] respectively, according to eqs 1 and 2

$$\text{HOMO} = -(E_{ox} + 4.75)\ (\text{eV}) \quad (1)$$

$$\text{LUMO} = -(E_{red} + 4.75)\ (\text{eV}) \quad (2)$$

The electrochemically determined energy gaps were deduced from the difference of the onset oxidation and reduction potentials. A summary of the redox potentials is provided in Table 1.

It can be seen from Figure 3 that there is one reversible n-doping/dedoping (reduction/reoxidation) process in the negative potential range for both compounds. There are also two reversible p-doping/dedoping (oxidation/reduction) processes in the positive potential range. For example, the half −wave potentials for oxidation (E_{ox}) and reduction (E_{red}) for DPPS are at 0.71 and −1.29 V, respectively. The electrochemical energy gap found for DPPS is 2.00 eV, which is similar to the value obtained from both the absorption spectra (Figure 4, Table 3) and DFT calculations. The oxidation and reduction potentials of these compounds can be adjusted by varying the number of selenophene units. As expected, compound DPPDS has a lower band gap than DPPS with an electrochemical band gap of 1.74 eV, with half-wave potentials of oxidation and reduction occurring at 0.64 V and −1.10 V, respectively. As a comparison, the thiophene-based material, SMDPPEH, has a HOMO level of −5.2 eV and LUMO level of −3.7 eV,[22] which is comparable to that of DPPDS.

4. Optical Properties. The absorption spectra for both solutions and thin films were obtained for each compound. These results are summarized in Table 3. As can be seen in Figure 4a, the chloroform solution absorption spectra of both compounds exhibit similar features. Two main absorption peaks appear in both the ultraviolet and visible parts of the spectrum from 300 to 450 nm and from 550 to 750 nm, respectively. The latter absorption band is attributed to the charge transfer band from the selenophene units to the DPP core. It should be noted that both compounds exhibit a broad band in the long wavelength regions. This is due to the intermolecular aggregation state caused by the strong polarity of the amide groups in the DPP units[39,40] as well as the increased vibronic coupling associated with the molecular rigidity imposed by molecular connectivity in solution measurements.[39]

Absorption maxima (λ_{max}) were observed at 628 nm in solution for both DPPS and DPPDS and the molar absorption coefficients in solution (ε_s) were calculated to be 61 300 M^{-1} cm^{-1} for DPPS and 76 100 M^{-1} cm^{-1} for DPPDS. Thin film absorption maxima were found at 695 nm for DPPS and 655 nm for DPPDS with calculated thin film molar absorption coefficients (ε_{tf}) of 32 000 and 35 400 M^{-1} cm^{-1} for DPPS and DPPDS, respectively. The addition of selenophene rings results in a

Table 1. Electrochemical Properties and Theoretical Calculations of DPPS and DPPDS

	electrochemistry data					DFT calculation		
	E_{ox} (V)	E_{red} (V)	HOMO (eV)	LUMO (eV)	E_g (eV)	HOMO (eV)	LUMO (eV)	E_g (eV)
DPPS	0.71	−1.29	−5.46	−3.46	2.00	−4.95	−3.05	1.90
DPPDS	0.64	−1.10	−5.39	−3.65	1.74	−4.87	−3.08	1.79

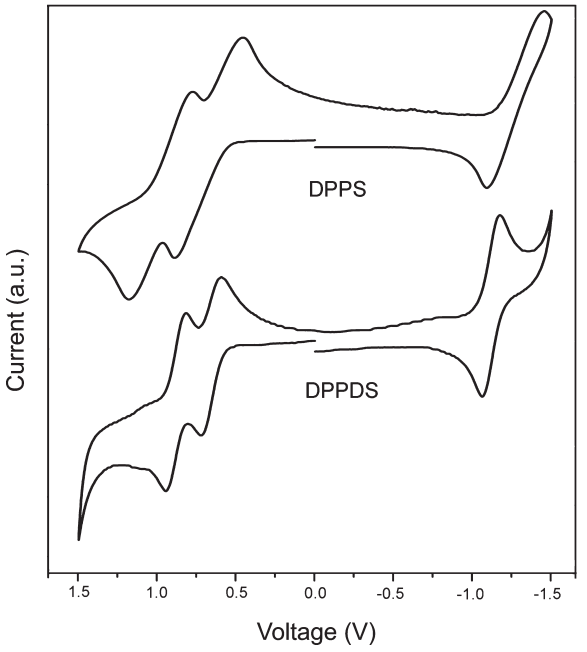

Figure 3. Cyclic voltammograms of DPPS and DPPDS in anhydrous dichloromethane solution containing 0.1 mol/L Bu_4NPF_6 at a scan rate of 100 mV/s.

red-shift of the absorption spectra due to an increase in the π-conjugation length. This is consistent with the red-shift observed for DPPDS compared to DPPS, as shown in Figure 4a. Specifically, the absorption maximum (λ_{max}) of the charge-transfer band is extended by 27 nm for DPPDS to longer wavelengths. The thin film absorption of DPPS and DPPDS on glass substrates (Figure 4b) exhibit a large red-shift compared to the solution spectra, suggesting an effective interchain $\pi-\pi$ stacking phenomena. The absorption bands edges extend up to 745 and 830 nm for DPPS and DPPDS, respectively. On the basis of the absorption spectra, the optical band gap was calculated to be 1.73 and 1.52 eV, respectively, for DPPS and DPPDS.

5. Photovoltaic Properties and Thin Film Morphology of DPPS and DPPDS. To demonstrate the potential of DPPS and DPPDS as electron donating chromophores, BHJ solar cells were fabricated. Figure 5 shows current density versus voltage ($J-V$) curves for DPPS and DPPDS devices fabricated under optimized conditions and characterized under simulated AM 1.5G solar radiation at an incident power intensity of 100 mW/cm^2. Table 4 provides a summary of the photovoltaic properties for the average 16 devices for DPPS and DPPDS fabricated under the optimized conditions. Each active layer blend was subjected to a series of device optimizations as described in the Experimental Section. Conditions examined included solvents, donor:acceptor weight ratios, and annealing times and temperatures. For both DPPS and DPPDS, the optimal device conditions were found to

Table 2. DFT computed Ground State Energies, Bond Lengths, Bond Angles, and Torsion Angles for DPPS, DPPDS, and SMDPPEH

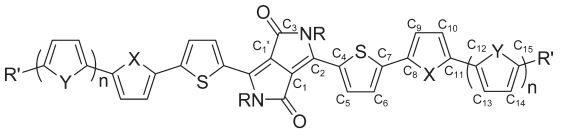

R = 2-ethylhexyl*, R' = tetradecyl*
DPPS : n = 0, X = Se
DPPDS : n = 1, X = Se, Y = Se
SMDPPEH : n = 1, X = S, Y = S

*methyl groups were used for calculation

	DPPS	DPPDS	SMDPPEH
energy (hartree)	−6857.8973	−11963.8936	−3559.1526
Bond Length (Å)			
C_1'-C_3	1.445	1.447	1.445
C_1'−C_1	1.419	1.421	1.417
C_1−C_2	1.398	1.390	1.398
C_2−N	1.395	1.409	1.400
C_3−O	1.230	1.228	1.229
C_2−C_4	1.434	1.435	1.435
C_4−C_5	1.391	1.393	1.393
C_4−S	1.766	1.759	1.761
C_5−C_6	1.405	1.407	1.406
C_6−C_7	1.386	1.387	1.386
C_7−C_8	1.440	1.438	1.448
C_8−C_9	1.376	1.375	1.381
C_9−C_{10}	1.424	1.418	1.415
Bond Angles (deg)			
C_1'−C_1−C_2	109.4	109.8	109.3
C_1−C_2−N	106.6	106.7	106.6
C_2−N−C_3	111.7	111.7	111.6
N−C_3−C_1'	103.9	104.1	103.9
C_3−C_1'−C_1	108.5	108.1	108.5
Dihedral Angles (deg)			
C_1−C_2−C_4−C_5	1.27	0.67	0.69
C_6−C_7−C_8−C_9	175.73	179.46	167.98
C_{10}−C_{11}−C_{12}−C_{13}		179.97	163.15

be 1:1 weight ratios of DPPS:$PC_{61}BM$ and DPPDS:$PC_{61}BM$ in chloroform, respectively, without annealing for DPPS and with annealing at 80 °C for 5 min for DPPDS. Devices made in $CHCl_3$ showed over 50% improvement in device performance compared to those devices made in *ortho*-dichlorobenzene (*o*DCB). In the PCBM concentration studies, the observed increase in PCEs with 1:1 weight ratios can be attributed to increased short circuit current density (J_{SC}) at this ratio, with decreasing J_{SC} at higher and lower

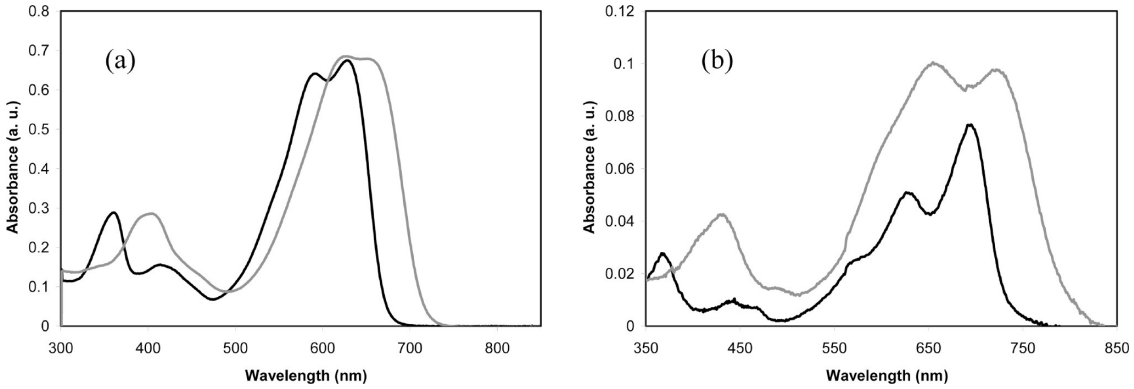

Figure 4. UV−vis absorption spectra of DPPS (black line) and DPPDS (gray line) in (a) $CHCl_3$ (0.0125 mg mL^{-1}) and (b) thin film on glass substrates.

Table 3. UV−Vis Absorption Optical Data of DPPS and DPPDS

	solution	film		
	λ_{max}(nm)	λ_{max}(nm)	λ_{onset}(nm)	$E_g{}^a$(eV)
DPPS	628	695	720	1.73
DPPDS	628	655, 722	815	1.52

[a] Calculated from the onset absorption of the compounds solution and film, $E_g = 1240/\lambda_{onset}$.

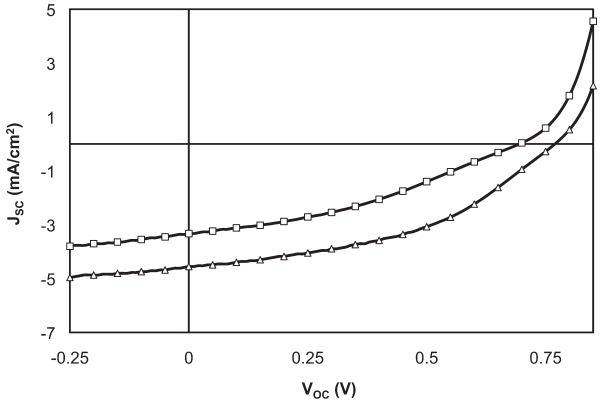

Figure 5. $J-V$ characteristics for solar cells prepared with an active layer of $PC_{61}BM$ and DPPS (triangle) or DPPDS (square) under simulated AM 1.5G irradiation (100 mW/cm^2).

weight ratios. With DPPS, annealing lowered the overall J_{SC} and resulting PCE, even at low temperatures. With DPPDS, annealing tended to show slight decreases in J_{SC}, but a concomitant increase in FF resulted in greater overall performance. These fabrication conditions resulted in average PCEs of 1.53 ± 0.04% for DPPS and 0.84 ± 0.04% for DPPDS. In our hands, when $PC_{71}BM$ was used as an acceptor, no improvement in PCE was observed.

The photovoltaic properties for DPPS are consistently higher than those of DPPDS, even though the greater π-conjugation length of DPPDS results in a broader absorption band that extends to the edge of the visible wavelengths and an increase in the molar absorptivity. The decrease in open circuit voltage (V_{OC}) with increasing selenophene content of the highest efficiency devices is consistent with the increasing HOMO levels of these molecules

Table 4. Photovoltaic Characteristics of Best Devices Made from Blends of DPPS or DPPDS and $PC_{61}BM$

	V_{OC} (mV)	J_{SC} (mA/cm^2)	FF	PCE (%)
DPPS	766 ± 13	4.9 ± 0.3	0.41 ± 0.02	1.53 ± 0.04
DPPDS	696 ± 16	3.4 ± 0.2	0.36 ± 0.01	0.84 ± 0.04

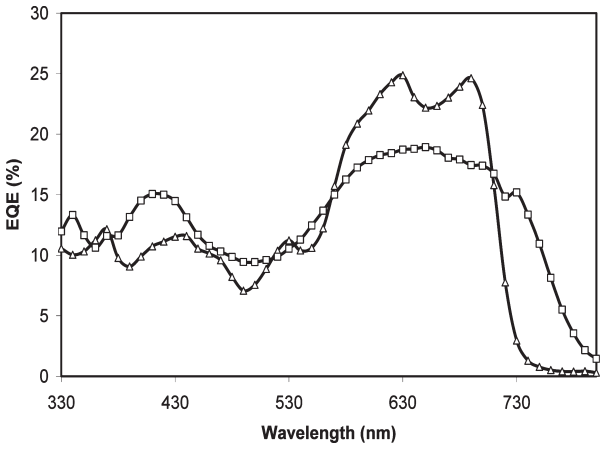

Figure 6. External quantum efficiency (EQE) curves for blends of DPPS:$PC_{61}BM$ (triangle) and DPPDS:$PC_{61}BM$ (square).

from −4.95 eV for DPPS to −4.85 eV for DPPDS. J_{SC} varies consistently with both the external quantum efficiency (EQE) and the mobility (μ) for each material. Figure 6 presents the EQE curves for devices fabricated with DPPS and DPPDS under optimized device performance conditions, with LiF/Al top contacts. Peak EQEs of approximately 25% at both 630 and 690 nm were found for DPPS. The EQE for DPPDS is significantly reduced to 19% at 650 nm. Hole-only mobilities of both materials were examined through organic thin film transistors (OTFTs) in the top contact geometry. DPPS had a hole mobility of 4×10^{-5} $cm^2/(V\,s)$ and DPPDS showed a hole mobility of 2×10^{-5} $cm^2/(V\,s)$. We attribute the lower PCE and EQE of the DPPDS devices, despite the extended absorption wavelength and greater absorption coefficient, to the lower hole mobility observed in the thin films. Our DFT calculations show that the DPPDS has the most planar structure, followed by DPPS, and finally SMDPPEH. Based on molecular packing, we would expect DPPDS to show the greatest hole

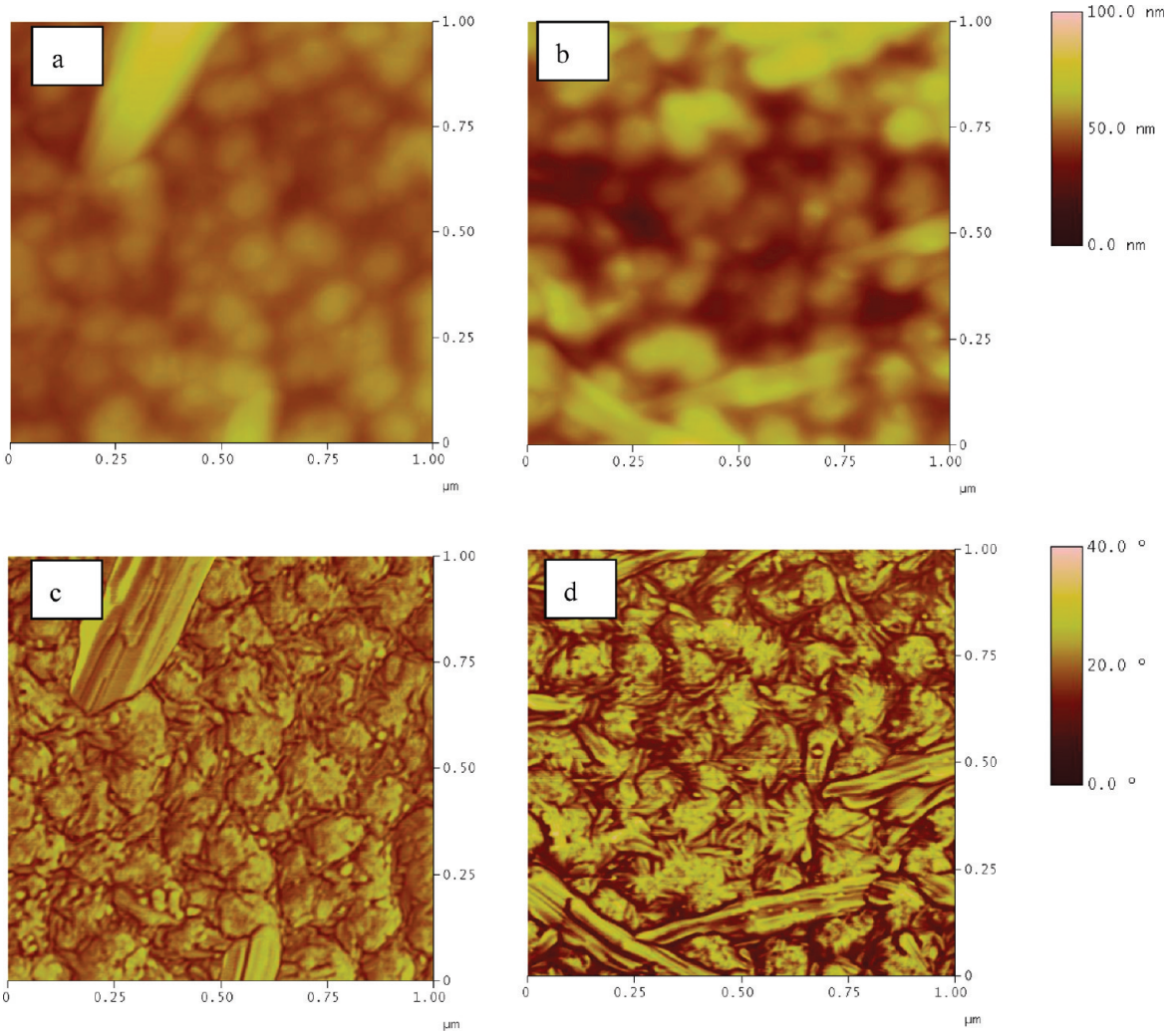

Figure 7. AFM height images of (a) DPPS:PCBM active layer between electrodes and (b) DPPDS:PCBM active layer between electrodes. AFM phase images of (c) DPPS:PCBM and (d) DPPDS:PCBM active layers.

mobility but the opposite trend is observed. The decreased mobility can be attributed to film morphology rather than molecular packing, where the formation of large crystallites leads to decreased uniformity and increased surface roughness in the thin film.[41] Increased grain boundaries may also play a role in the poor OTFT performances.[41]

The thin film morphology of the OPV active layer was also considered for discussion of the lower PCE of DPPDS as it is known to affect the overall device performance in BHJ solar cells. As can be seen in Figure 7, both active layers have similar morphologies with domains around 100 nm in diameter, and both are characterized by high rms roughness values of 10 nm for DPPS and 9 nm for DPPDS. The large domains and high rms roughness values may limit the overall device performance of our selenophene derivatives as compared to the SMDPPEH analog of Nguyen, et al.,[22] as the domains are larger than the optimal separation required for efficient exciton diffusion. Future investigation of solvent mixtures may help improve the morphology of the active layers.

CONCLUSION

The synthesis and characterization of novel low-band-gap oligoselenophenes functionalized with a diketopyrrolopyrrole core was presented; to date, these are the first reported oligoselenophenes used in molecular bulk heterojunction solar cells. These chromophores exhibit a broad optical absorption which is induced by the internal electron transfer between the selenophenes and the DPP core. Solar cells fabricated with DPPS and DPPDS show peak EQEs of 25% and 19%, and OTFT hole mobilities of 4×10^{-5} cm^2/(V s) and 2×10^{-5} cm^2/(V s), respectively. Under optimized fabrication conditions, solar cells consisting of an active layer of DPPS:$PC_{61}BM$ and DPPDS:$PC_{61}BM$ resulted in average PCEs of 1.53 ± 0.04% and 0.84 ± 0.04%. Further improvements to the overall device efficiencies may be realized through the optimization of film morphology to improve hole mobilities as well as charge dissociation.

EXPERIMENTAL SECTION

Materials and Characterization. ^{1}H NMR and ^{13}C NMR spectra were collected on a Bruker Avance DPS-300 spectrometer, respectively. Mass Spectrometry was performed by Hewlett-Packard 5971A Gas Chromatograph and Bruker Biflex III MALDI-TOF (both positive and negative ion reflector mode). The absorption spectra were measured on a Perkins-Elmer Lambda-9 spectrophotometer. Unless otherwise stated, reagents were commercially obtained and use without further

purification. Dry THF and toluene were obtained from an Innovative Technology, Inc. Pure Solv MD-2 solvent purification system 3,6-bis-(5-bromothiophen-2-yl)-2,5-Diethylhexyl-pyrrolo-[3,4-c]-pyrrole-1,4-dione[42] and 2-bromo- selenophene[43] were synthesized according to the literature.

Density Functional Theory (DFT). DFT calculations were performed using the Gaussian 03 software package at the B3LYP/6-31G(d) level. The HOMO and LUMO energies were determined using minimized singlet geometries to approximate to the ground state. Geometry optimization followed by frequency calculation was performed to obtain the lowest energy conformer.

Electrochemistry. Cyclic voltammetry measurements were carried out using a Bioanalytical System (BAS) Epsilon potentiostat equipped with a standard three-electrode configuration. Typically, a three-electrode cell equipped with a glassy carbon working electrode, a Ag/AgCl reference electrode, and a Pt wire counter electrode was employed. The measurements were performed in anhydrous dichloromethane with tetrabutylammonium hexafluorophosphate (0.1 M) as the supporting electrolyte under a nitrogen atmosphere, at a scan rate of 100 mV/S.

Synthesis. The synthetic routines of the target compounds are shown in Scheme 1. The detailed synthetic processes are as follows.

1-(Selenophen-2-yl)-tetradecan-1-one (2). Myristoyl chloride (741.2 mg, 3.1 mmol) was added to a solution of selenophene (**1**) (393.4 mg, 3.1 mmol) in anhydrous CH_2Cl_2. The solution was stirred at room temperature for 30 min, then cooled to 0 °C. To the solution was carefully added $AlCl_3$ (532.4 mg, 4.0 mmol) for 5 min. After the addition was complete, the mixture was stirred in an ice-bath for another 3 h. Water was added to the system to quench the reaction then extracted with CH_2Cl_2. The combined organic phases were dried with anhydrous Na_2SO_4 and the solvent was removed under vacuum. The crude residue was purified by silica gel chromatography (CH_2Cl_2), yielding a yellowish liquid (728.4 mg, 71% yield). ^{1}H NMR (300 MHz, $CDCl_3$): 8.41 (d, 1H, J = 4.8 Hz), 8.06 (d, 1H, J = 5.2 Hz), 7.32 (t, 1H, J = 5.0 Hz), 2.92 (t, 2H, J = 6.8 Hz), 1.42−1.29 (m, 16H), 0.92−0.81 (m, 9H). ^{13}C NMR (75 MHz, $CDCl_3$): 197.3, 154.7, 136.2, 131.1, 127.4, 47.6, 32.4, 29.6, 29.5, 29.3, 23.4, 22.5, 14.3. MS (EI) m/z calcd, 341.4; found, 341.1.

2-Tetradecylselenophene (3). $AlCl_3$ (2.66 g, 20 mmol) was carefully added to a solution of $LiAlH_4$ (1.06 g, 28 mmol) in anhydrous ether at 0 °C, then 1-(selenophen-2-yl)-tetradecan-1-one (**2**) (1.03 g, 3 mmol) in 10 mL anhydrous ether was added to the resulting suspension. The mixture was warmed to room temperature and stirred for another 3 h. After the reaction was complete, ice was carefully added to the system to quench the reaction. The precipitate was filtered off and washed with ether. The combined filtrate was washed with water and extracted with CH_2Cl_2. After removing the solvent, the crude product was purified by silica gel chromatography (CH_2Cl_2), yielding a light yellow liquid (540 mg, 55% yield). ^{1}H NMR (300 MHz, $CDCl_3$): 7.71 (d, 1H, J = 5.2 Hz), 7.10 (t, 1H, J = 5.0 Hz), 6.92 (d, 1H, J = 5.4 Hz), 2.01 (t, 2H, J = 6.6 Hz), 1.62 (m, 2H), 1.40−1.27 (m, 16H), 0.93−0.82 (m, 9H). ^{13}C NMR (75 MHz, $CDCl_3$): 135.1, 134.8, 128.6, 128.1, 44.3, 31.6, 30.9, 29.7, 29.6, 29.3, 23.2, 14.3. MS (EI) m/z calcd, 327.4; found, 326.2.

2-Trimethyltin-5-Tetradecylselenophene (4). 2-Tetradecylselenophene (**3**) (654.3 mg, 2.1 mmol) and 10 mL anhydrous THF was added into a flask under nitrogen atmosphere. N-butyllithium (0.8 mL, 2.5 mol/L) was added dropwise into the solution at −78 °C. The mixture was stirred at this temperature for another hour, then trimethyltin chloride (2 mL, 2 mmol/mL) was added in one portion; the reactant turned clear rapidly. The resulting solution was stirred overnight at room temperature then the reaction was terminated by adding water. The mixture was extracted with CH_2Cl_2 and dried with anhydrous Na_2SO_4. After the solvent was removed, the product was a light yellow liquid (880.1 mg, 90% yield). ^{1}H NMR (300 MHz, $CDCl_3$): 7.15 (d, 1H, J = 5.8 Hz), 6.92 (d, 1H, J = 5.7 Hz), 2.01 (t, 2H, J = 6.4 Hz), 1.61 (m, 2H), 1.40−1.27 (m, 16H), 0.93−0.86 (m, 9H), 0.84 (s, 9H). MS (EI) m/z calcd, 490.2; found, 490.6.

5-Tetradecyl-2,2′-biselenophene (5). 2-Trimethyltin-5-tetradecylselenophene (**4**) (640 mg, 1.3 mmol) and 2-bromoselenophene (273 mg, 1.3 mmol) were mixed in 20 mL of anhydrous toluene under a nitrogen atmosphere, and the resulting solution was degassed for 10 min. The catalyst $Pd(PPh_3)_2Cl_2$ (18 mg, 0.026 mmol) was added to the solution and the mixture was refluxed under nitrogen overnight. After the reaction was complete, the solvent was removed under a vacuum, and the crude residue was purified by silica gel chromatography (CH_2Cl_2), yielding a light yellow solid (984 mg, 83% yield). ^{1}H NMR (300 MHz, $CDCl_3$): 7.78 (d, 1H, J = 5.5 Hz), 7.21 (d, 1H, J = 5.7 Hz), 7.18 −7.14 (m, 2H), 6.84 (d, 1H, J = 5.5 Hz), 2.03 (t, 2H, J = 6.7 Hz), 1.61 (m, 2H), 1.41−1.25 (m, 16H), 0.91−0.81 (m, 9H). ^{13}C NMR (75 MHz, $CDCl_3$): 143.2, 142.7, 136.2, 134.5, 130.2, 129.4, 119.3, 119.1, 43.6, 33.6, 31.2, 29.7, 29.5, 29.4, 22.6, 14.5. MS (EI) m/z calcd, 456.4; found, 455.6.

5-Trimethyltin-5′-Tetradecyl-2,2′-biselenophene (6). 5-Tetradecyl-2,2′-biselenophene (**5**) (730 mg, 1.6 mmol) and 20 mL anhydrous THF was added into a flask under nitrogen atmosphere. N-butyllithium (0.64 mL, 2.5 mol/L) was added dropwise to the solution at −78 °C. The mixture was stirred at this temperature for 1 h, then trimethyltin chloride (1.6 mL, 1 mol/L) was added in one portion; the reactant turned clear rapidly. The resulting solution was stirred overnight at room temperature then the reaction was terminated by adding water. The mixture was extracted with CH_2Cl_2 and dried with anhydrous Na_2SO_4. After removing the solvent, the product was a light yellow liquid (813 mg, 82%). ^{1}H NMR (300 MHz, $CDCl_3$): 7.10 (d, 2H, J = 5.3 Hz), 7.04 (d, 1H, J = 5.1 Hz), 6.87 (d, 1H, J = 5.0 Hz), 2.03 (t, 2H, J = 6.8 Hz), 1.63 (m, 2H), 1.40−1.25 (m, 16H), 0.97−0.88 (m, 9H), 0.83 (s, 9H). MS (MALDI-TOF) m/z calcd, 619.2; foun,d 618.6

General Synthesis (DPPS and DPPDS). In an oven-dried Schlenk flask, 3,6-bis-(5-bromothiophen-2-yl)-2,5-diethylhexyl-pyrrolo-[3,4-c]-pyrrole-1,4-dione and the appropriate trimethyltin-oligoselenophene compound were dissolved in 20 mL of anhydrous toluene. The resulting solution was degassed for 15 min. $Pd(PPh_3)_2Cl_2$ was added to the mixture and the mixture was degassed for another 5 min. The resulting solution was stirred and refluxed under nitrogen overnight. After the reaction was complete, water was added to the mixture to quench the reaction. The mixture was washed with water and extracted with CH_2Cl_2 twice. The combined organic phases were dried with anhydrous Na_2SO_4 and the solvent was removed under a vacuum. The crude product was purified by silica gel chromatography (CH_2Cl_2) to obtain the pure product.

DPPS. DPPS is formed as a deep red powder (yield: 63%). ^{1}H NMR (300 MHz, $CDCl_3$): 7.76 (d, 2H, J = 5.8 Hz), 7.52 (d, 2H, J = 5.2 Hz), 7.31 (d, 2H, J = 5.7 Hz), 6.94 (d, 2H, J = 5.3 Hz), 4.09 (m, 4H), 2.06 (t, 4H, J = 6.7 Hz), 1.87 (m, 2H), 1.70 (m, 4H), 1.41−1.03 (m, 64H), 0.93−0.88 (m, 12H). ^{13}C NMR (75 MHz, $CDCl_3$): 173.2, 143.4, 141.6, 137.2, 132.8, 130.6, 129.4, 128.1, 115.4, 48.1, 45.6, 37.9, 32.4, 31.1, 29.8, 29.6, 29.3, 26.4, 23.2, 22.1, 14.5, 11.9. MS (MALDI-TOF) m/z calcd for $C_{66}H_{100}N_2O_2S_2Se_2$, 1175.6; found, 1176.4

DPPDS. DPPDS is formed as a deep blue powder (yield: 47%). ^{1}H NMR (300 MHz, $CDCl_3$): 7.78 (d, 2H, J = 6.1 Hz), 7.51 (d, 2H, J = 5.3 Hz), 7.32 (d, 2H, J = 5.9 Hz), 7.17−7.11 (m, 4H), 6.92 (d, 2H, J = 5.1 Hz), 4.11 (m,4H), 2.11 (t, 4H, J = 6.8 Hz), 1.89 (m, 2H), 1,72 (m, 4H), 1.43- 1.08 (m, 64H), 0.94−0.85 (m, 12H). ^{13}C NMR (75 MHz, $CDCl_3$): 172.5, 143.1, 142.7, 141.5, 141.3, 137.3, 133.1, 131.5, 129.1, 128.7, 126.4, 117.2, 50.2, 47.3, 38.6, 33.2, 31.8, 29.5, 29.3, 29.1, 27.2, 22.8, 21.71, 15.6, 13.1. MS (MALDI-TOF) m/z calcd for $C_{66}H_{100}N_2O_2S_2Se_2$, 1433.6; found, 1157.4 [$M + Na^+$].

Device Fabrication. ITO-coated glass substrates (15 Ωm^{-2}) were cleaned with Meri Suds detergent, DI water, acetone, and IPA in an ultrasonic bath for 10 min each. They were then dried under N_2 and air

plasma cleaned for 15 min. A 40 nm layer of poly(3,4-ethylenedioxythiophene) poly(styrenesulfonate) (PEDOT:PSS; clevios PVP Al 4083) was spin-coated as the hole selective layer and annealed at 120 °C for 10 min. Active layers consisting of DPPS or DPPDS and phenyl-C_{61}-butyric acid methyl ester (American Dye Source, Inc. ADS61BFB) with various weight ratios (1:3, 1:2.5, 1:2, 1:1.5, 1:1, 1:0.8, 1:0.6) in chloroform (20 mg mL^{-1}) were spin-coated on top of the PEDOT:PSS at 1500 rpm for 60 s. All active layer solutions were allowed to stir in a glovebox for at least 4 h at room temperature before being filtered with a 0.2 μm PTFE filter. Top contacts for photovoltaic and EQE measurements consisted 0.9 nm LiF and 100 nm Al layers that were thermally deposited at a base pressure of 2×10^{-6} Torr. Photovoltaic devices were annealed for 2, 5, 10, and 15 min at 40, 50, 60, 80, and 100 °C in order to determine the optimal device performance conditions.

For OTFT measurements, devices were fabricated with a top contact geometry on heavily doped p-type Si/SiO_2 wafers (300 nm thermal oxide, Montco Silicon Technologies, Inc.). Substrates were cleaned by sonicating in acetone, methanol, and IPA for 15 min each. The wafers were then dried under nitrogen and air plasma etched for 10 min. Solutions of DPPS and DPPDS were made with chloroform ($CHCl_3$), *o*-dichlorobenzene (*o*DCB), and chlorobenzene (CB) at concentrations of 5 mg/mL. $CHCl_3$ solutions were spin-coated at 800 rpm, whereas *o*DCB and CB solutions were spin-coated at 1200 rpm, all for 60 s. Au source and drain electrodes (W = 9000 μm, L = 900 μm) were thermally evaporated through a shadow mask to 50 nm thick at a base pressure of 7×10^{-7} Torr.

Device Characterization. Photovoltaic device performance was characterized in air under simulated 100 mW cm^{-2} AM1.5G irradiation using an Oriel Xe arc lamp coupled with a Keithley 2400 source measurement unit. The solar simulator light intensity was calibrated with an NREL certified Si photodiode with a KG5 optical filter. The EQE was measured using the same source for photovoltaic measurements along with and Oriel Cornerstone 130 1/8 m monochromator and referenced to an unfiltered, NREL certified Si photodiode. OTFT measurements were conducted in the dark in inert atmosphere.

AUTHOR INFORMATION

Corresponding Author

*E-mail: luscombe@u.washington.edu.

ACKNOWLEDGMENT

This work was supported by the NSF (STC-MDITR DMR 0120967 and CAREER Award DMR 0747489) and the DOE Solar America Initiative.

REFERENCES

(1) Krebs, F. C. *Sol. Energy Mater. Sol. Cells* **2009**, *93*, 393.
(2) Thompson, B. C.; Fréchet, J. M. J. *Angew. Chem., Int. Ed.* **2008**, *47*, 58.
(3) Yu, G.; Gao, J.; Hummelen, J. C.; Wudl, F.; Heeger, A. J. *Science* **1995**, *270*, 1789.
(4) Liang, Y. Y.; Wu, Y.; Feng, D. Q.; Tsai, S. T.; Son, H. J.; Li, G.; Yu, L. P. *J. Am. Chem. Soc.* **2009**, *131*, 56.
(5) Peet, J.; Kim, J. Y.; Coates, N. E.; Ma, W. L.; Moses, D.; Heeger, A. J.; Bazan, G. C. *Nat. Mater.* **2007**, *6*, 497.
(6) Piliego, C.; Holcombe, T. W.; Douglas, J. D.; Woo, C. H.; Beaujuge, P. M.; Fréchet, J. M. J. *J. Am. Chem. Soc.* **2010**, *132*, 7595.
(7) Qin, R. P.; Li, W. W.; Li, C. H.; Du, C.; Veit, C.; Schleiermacher, H. F.; Andersson, M.; Bo, Z. S.; Liu, Z. P.; Inganäs, O.; Wuerfel, U.; Zhang, F. L. *J. Am. Chem. Soc.* **2009**, *131*, 14612.
(8) Chen, H. Y.; Hou, J. H.; Zhang, S. Q.; Liang, Y. Y.; Yang, G. W.; Yang, Y.; Yu, L. P.; Wu, Y.; Li, G. *Nat. Photonics* **2009**, *3*, 649.
(9) Scharber, M. C.; Wuhlbacher, D.; Koppe, M.; Denk, P.; Waldauf, C.; Heeger, A. J.; Brabec, C. L. *Adv. Mater.* **2006**, *18*, 789.
(10) Chen, C. P.; Chan, S. H.; Chao, T. C.; Ting, C.; Ko, B. T. *J. Am. Chem. Soc.* **2008**, *130*, 12828.
(11) Wang, E. G.; Wang, L.; Lan, L. F.; Luo, C.; Zhuang, W. L.; Peng, J. B.; Cao, Y. *Appl. Phys. Lett.* **2008**, *92*, 33307.
(12) Wu, P. T.; Bull, T.; Kim, F. S.; Luscombe, C. K.; Jenekhe, S. A. *Macromolecules* **2009**, *42*, 671.
(13) Xiao, S. Q.; Zhou, H. X.; You, W. *Macromolecules* **2008**, *41*, 5688.
(14) Yang, P. Y.; Zhou, X.; Cao, G.; Luscombe, C. K. *J. Mater. Chem.* **2010**, *20*, 2612.
(15) Zhang, Y.; Hau, S.; Yip, H.; Sun, Y.; Acton, O.; Jen, A. K. Y. *Chem. Mater.* **2010**, *22*, 2696.
(16) Zhou, E. J.; Yamakawa, S.; Zhang, Y.; Tajima, K.; Yang, C. H.; Hashimoto, K. *J. Mater. Chem.* **2009**, *19*, 7730.
(17) Schmidt-Mende, L.; Fechtenkotter, A.; Mullen, K.; Moons, E.; Friend, R. H.; MacKenzie, J. D. *Science* **2001**, *293*, 1119.
(18) Sun, M. L.; Wang, L.; Zhu, X. H.; Du, B.; Liu, R.; Yang, W.; Cao, Y. *Sol. Energy Mater. Sol. Cells* **2007**, *91*, 1681.
(19) Tamayo, A. B.; Walker, B.; Nguyen, T. Q. *J. Phys. Chem. C* **2008**, *112*, 11545.
(20) Dang, X. D.; Tamayo, A. B.; Seo, J.; Hoven, C. V.; Walker, B.; Nguyen, T. Q. *Adv. Funct. Mater.* **2010**, *20*, 3314.
(21) He, C.; He, Q. G.; Yang, X. D.; Wu, G. L.; Yang, C. H.; Bai, F. L.; Shuai, Z. G.; Wang, L. X.; Li, Y. F. *J. Phys. Chem. C* **2007**, *111*, 8661.
(22) Tamayo, A. B.; Dang, X. D.; Walker, B.; Seo, J.; Kent, T.; Nguyen, T. Q. *Appl. Phys. Lett.* **2009**, *94*, 103301.
(23) Patra, A.; Bendikov, M. *J. Mater. Chem.* **2010**, *20*, 422.
(24) Chen, Z. Y.; Lemke, H.; Albert-Seifried, S.; Caironi, M.; Nielsen, M. M.; Heeney, M.; Zhang, W. M.; McCulloch, I.; Sirringhaus, H. *Adv. Mater.* **2006**, *22*, 2371.
(25) Cho, N. S.; Lee, S. K.; Seo, J. H.; Elbing, M.; Azoulay, J. D.; Park, J.; Cho, S.; Heeger, A. J.; Bazan, G. C. *J. Mater. Chem.* **2008**, *18*, 4909.
(26) Gao, F. F.; Cheng, Y. M.; Yu, Q. J.; Liu, S.; Shi, D.; Li, Y. H.; Wang, P. *Inorg. Chem.* **2009**, *48*, 2664.
(27) Kong, H.; Jung, Y. K.; Cho, N. S.; Kang, I. N.; Park, J. H.; Cho, S.; Shim, H. K. *Chem. Mater.* **2009**, *21*, 2650.
(28) Bijleveld, J. C.; Zoombelt, A. P.; Mathijssen, S. G. J.; Wienk, M. M.; Turbiez, M.; de Leeuw, D. M.; Janssen, R. A. J. *J. Am. Chem. Soc.* **2009**, *131*, 16616.
(29) Wienk, M. M.; Turbiez, M.; Gilot, J.; Janssen, R. A. J. *Adv. Mater.* **2008**, *20*, 2556.
(30) Zou, Y. P.; Gendron, D.; Badrou-Aich, R.; Najari, A.; Tao, Y.; Leclerc, M. *Macromolecules* **2009**, *42*, 2891.
(31) Nelson, T. L.; Young, T. M.; Liu, J.; Mishra, S. P.; Belot, J. A.; Balliet, C. L.; Javier, A. E.; Kowalewski, T.; McCullough, R. D. *Adv. Mater.* **2010**, *22*, 4617.
(32) Bijleveld, J. C.; Gevaerts, V. S.; Nuzzo, D. D.; Turbiez, M.; Mathijssen, S. G. J.; de Leeuw, D. M.; Wienk, M. M.; Janssen, R. A. J. *Adv. Mater.* **2010**, *22*, E242.
(33) Woo, C. H.; Beaujuge, P. M.; Holcombe, T. W.; Lee, O. P.; Fréchet, J. M. J. *J. Am. Chem. Soc.* **2010**, *132*, 15547.
(34) Tamayo, A. B.; Tantiwiwat, M.; Walker, B.; Nguyen, T. Q. *J. Phys. Chem. C* **2008**, *112*, 15543.
(35) Luňák, S., Jr.; Vyňuchal, J.; Hrdina, R. *J. Mol. Struct.* **2009**, *919*, 239.
(36) Milliefiori, S.; Alparone, A. *Synth. Met.* **1998**, *95*, 217.
(37) Milliefiori, S.; Alparone, A. *J. Heterocyclic Chem.* **2000**, *37*, 847.
(38) Gagne, R. R.; Koval, C. A.; Lisensky, G. C. *Inorg. Chem.* **1980**, *19*, 2854.
(39) Huo, L. J.; Hou, J. H.; Chen, H. Y.; Zhang, S. Q.; Jiang, Y.; Chen, T. L.; Yang, Y. *Macromolecules* **2009**, *42*, 6564.
(40) Wallquist, O.; Lenz, R. *Macromol. Symp.* **2002**, *187*, 617.
(41) Smith, J.; Heeney, M.; McCulloch, I.; Nekuda Malik, J.; Stingelin, N.; Bradley, D. D. C.; Anthopoulos, T. D. *Org. Electron.* **2010**, *12*, 143.
(42) Zhou, E. J.; Yamakawa, S. P.; Tajima, K.; Yang, C. H.; Hashimoto, K. *Chem. Mater.* **2009**, *21*, 4055.
(43) Yang, R. Q.; Tian, R. Y.; Yan, J. G.; Zhang, Y.; Yang, J.; Hou, Q.; Yang, W.; Zhang, C.; Cao, Y. *Macromolecules* **2005**, *38*, 244.